Applied Catalysis B: Environmental 204 (2017) 421–429

Contents lists available at ScienceDirect

Applied Catalysis B: Environmental

journal homepage: www.elsevier.com/locate/apcatb

Design of active Pt on TiO_2 based nanofibrous cathode for superior PEMFC performance and durability at high temperature

Yunseong Ji[a,1], Yong il Cho[a,1], Yukwon Jeon[a], Chanmin Lee[b], Dae-Hwan Park[a], Yong-Gun Shul[a,*]

[a] Department of Chemical and Biomolecular Engineering, Yonsei University, Seoul 120-749, Korea
[b] Center of Advanced Instrumental Analysis, Kyushu University, Kasuga, Fukuoka, 816-8580, Japan

ARTICLE INFO

Article history:
Received 16 June 2016
Received in revised form 27 October 2016
Accepted 23 November 2016
Available online 25 November 2016

Keywords:
Fuel cells
Composite materials
Nanofibers
Charge transport
Electronic structures

ABSTRACT

Oxygen reduction reaction (ORR) activity and stability of the cathode catalyst are important issues for practical applications, which should be even considered for the materials in high temperature polymer electrolyte membrane fuel cells (HT-PEMFCs). To improve these properties, modification of the catalyst electronic structure and finding durable supports can be a good approach. In this study, we synthesized a noble nanofibrous composite electrode which consist of carbon nanotube (CNT)-winded Pt/TiO_2 nanofiber (CNT-Pt/TiO_2). Our approach takes advantages of the electrochemical conductivity of CNF as well as better stability from the corrosion resistivity of TiO_2 and strong metal-support interaction (SMSI) between the Pt nanoparticles and TiO_2 nanofibers for less Pt dissolution. We also found that the Pt electronic state can be changed by an interaction with neighbouring CNT and TiO_2, resulting a decrease of Pt d-band vacancy for enhanced catalytic activity. Furthermore, nanofibrous structure with a unique 3D pore structure provides higher surface area for additional improvements of the mass transfer. These results reveal that the CNT-Pt/TiO_2 nanofiber based electrode shows enhanced performance with the maximum power density of 567 mW cm^{-2} compare to commercial Pt/C (461 mW cm^{-2}) with a significant durability at harsh conditions of 120 °C and RH 40%.

© 2016 Elsevier B.V. All rights reserved.

1. Introduction

Fuel cell is one of the most promising electrochemical energy conversion devices which withholds many advantages; high efficiency, high power density, rapid start up, any significant pollutant, etc. Especially, PEMFCs get a lot of attention because it has high power density and is relatively portable [1,2]. Primitive PEMFCs are usually operated at low temperatures (LT-PEMFC, ≤100 °C) [3]. However, these days, many researches in the field take an interest of high temperature PEMFC (HT-PEMFC, ≥100 °C) that offers several improvements such as high fuel cell efficiency, kinetics of oxygen reduction reactions, water management and tolerance to contaminants [4]. These factors can provide an efficiency and simplification of the system, and makes the system cost effective. However, still, there are many problems to commercialize the HT-PEMFC, for example catalysts with highly active and durable system.

Regardless of whether low or high temperature, platinum deposited on carbon material is a common PEMFC catalyst that has large surface area, high electrical conductivity, and appropriate pore structure [5]. However, carbon support materials usually suffer from degradation in a harsh PEMFC operation conditions [6]. Generally, carbon corrosion is occurred on the surface and it makes vacancies under the Pt nanoparticles. This mechanism gives rise to agglomeration and sinter of Pt particles via Ostwald ripening. Consequentially, carbon corrosion brings decreases of the electrochemical surface area (ECSA) and hinder long-term operations [7–9]. Thus, electrochemically stable support materials need to be developed [10].

Metal oxide supports can be an effective alternative for the electrode catalyst due to their excellent mechanical strength, corrosion resistance and inherently higher stability in various operation conditions than carbon. Through a theoretical calculation by K. Sasaki, titanium dioxide (TiO_2) can be one of the support candidates for fuel cell catalysts [11]. It has been attracted due to not only their low price for commercial availability but also their SMSI effect for better durability even under the acidic [12,13]. In addition, when the metal is loaded on TiO_2 surface, there are electron charge transfer from a TiO_2 to Pt, which provides an increase of the Pt electron

* Corresponding author.
E-mail address: shulyg@yonsei.ac.kr (Y.-G. Shul).
[1] These authors contributed equally to this work.

http://dx.doi.org/10.1016/j.apcatb.2016.11.053
0926-3373/© 2016 Elsevier B.V. All rights reserved.

density. This Pt electronic structure modification provides a relatively improved ORR activity that can be obtained comparing to the Pt on carbon supports [14–16]. However, pure TiO_2 is known as a semiconductor with a lack of electrical conductivity due to high band gap, resulting that the surface absorbed hydroxyls (OHs) hardly obtain electrons for ORR [12,13]. This is considered to be the main obstacle for using oxide materials directly as a support material. Therefore, we need a new effective cathode structure to induce platinum to an active state and boost up the electrical conductivity.

Herein, we report a detail investigation of a nanofibrous electrode by a CNT-Pt/TiO_2 nanofiber catalyst, which showed an exceptional HT-PEMFC performance and durability. In this 3D reticular electrode, CNTs boost up the electrical conductivity and donate electrons to the platinum on the Pt/TiO_2. In addition, the nanofibrous structure by using electrospun nanofiber nonwoven matrix has been shown to be useful as supports due to a greater surface-to-volume ratio and a 3D open structure that allows its surface active sites to be accessible for reactants more easily and effectively [17–19]. Finally, our new catalyst system for the attempt to replace the original Pt/C catalyst shows exceptional HT-PEMFC performance and it indicate the feasibility of our catalyst for an adoptable alternative.

2. Experimental section

2.1. Synthesis of TiO_2 nanofiber

TiO_2 nanofiber was prepared by electrospinning method. Electrospinning solution was prepared by dissolving Poly (vinyl pyrrolidine) (PVP, Mw = 1,300,000) (Aldrich) in Ethanol (Duksan) with a weight ratio of 1:10 for both guide polymer and viscoelasticity enhancer. It was stirred for 3 h to achieve complete dissolution and mixing. The solution further mixed with a weight rate of 1:0.2:0.05 for Titanium isopropoxide (Aldrich) and acetic acid (Duksan). Acetic acid acts as a Ti precursor protecting agent. After 3 h, a viscous solution is obtained. The solution was charged in a syringe and delivered at a constant flow rate of 30 $\mu m\ min^{-1}$. A high voltage of 15 kV was applied to the solution and a 30 gauge plastic nozzle tip was used. The distance from the tip to the collector was 15 cm. The chamber's condition was 25–30 °C and RH 20–30%. Then, the electro-spun nanofibers were heat-treated at 500 °C (1 °C min^{-1}) for 6 h to remove the PVP and obtain TiO_2 nanofiber with an anatase phase [17–19].

2.2. Preparation of CNT modified Pt/TiO_2 nanofiber catalyst

The Pt/TiO_2 nanofiber catalyst was synthesized by using Microwave-assisted polyol process to deposit the Pt nanoparticles. First, we dispersed the TiO_2 nanofibers in Ethylene glycol (EG, Duksan) and dissolved hexachloroplatinic acid ($H_2PtCl_2{\cdot}6H_2O$, Kojima Chemicals) with the pH value of 11 by adding 1 M NaOH (Duksan) solution drop by drop. After 1 h, Teflon vessel was filled with the solution and placed in a microwave oven (800W). Obtained powder was filtered dried for 8 h at 80 °C vacuum oven [20,21]. The Pt loading was fixed to 40 wt.% for the Pt/TiO_2 nanofiber catalyst. Finally, we produce a nanofibrous electrode by a modification of CNTs (Hanwha-nanotech, CM-100) around the Pt/TiO_2 nanofibers by filtrating different ratio of CNTs to enhance the surface area and electrical conductivity.

2.3. Material characterizations

Physical properties of the prepared TiO_2 nanofibers and CNT added catalysts were characterized by Powder X-ray diffraction (XRD), scanning electron microscope (SEM), Energy-dispersive X-ray spectroscopy (EDS), transmission electron microscopy (TEM), X-ray photoelectron spectroscopy (XPS) and X-ray absorption spectroscopy (XAS) were used. The SEM analysis was used to observe the morphologies of catalysts and EDS was introduced to obtain the loading amount of platinum. XRD patterns of the prepared catalysts were measured by X-ray diffractometer (Rigaku, Miniflex) with Cu Kα source at room temperature. The d-space of platinum and particle sizes before and after the tests were evaluated by TEM (JEOL, JEM-ARM 200F). Samples were prepared by ultrasonically suspending the NPs in ethanol; the suspension was then applied to a copper grid and dried in an oven. The chemical states of Pt 4f, Ti 2p, and O 1 s in the catalysts were estimated by the XPS spectra (Thermo Fisher Scientific, K-alpha) using mono Al Kα source. The XPS binding energies were referred to that of C 1 s in a graphitic state (284.8 eV). The XAS results were recorded at the Pohang Accelerator Laboratory (PAL), beamline 10C (Multipole-wiggler, Ge 13-element detector) and 10D (Bending magnet, Phoibos 150). Measurements were made at room temperature with solid samples. The spectra for the L_{III} edge of Pt were taken in transmission mode with separate He-filled IC Spec ionization chambers for incident and transmitted beams. And, to obtain additional evidences for the synergistic effect, O K-edge and Ti L_{III}-edge spectra were also observed [22].

2.4. Electrochemical characterizations

The electrochemical properties of the electrocatalyst were characterized by using three electrode system with a rotating disk electrode system (Pine Instruments). The system consisted of a glassy carbon working electrode, platinum wire counter electrode and standard calomel reference electrode (SCE, 0.24 V vs. RHE). Catalyst inks were prepared by ultrasonicating mixing of ethanol (1 ml), 5 wt.% Nafion solution (80 μl), and catalyst powder (0.01 g). The prepared inks were deposited on a glassy-carbon electrode and dried at room temperature in ambient air. The Pt loading was calculated from the amount of platinum in catalyst.

In order to examine the electrocatalyst properties, cyclic voltammetry (CV, 0.05–1.2 V vs SHE., 50 mV s^{-1}, N_2) and linear sweep voltammetry (LSV, 10 mV s^{-1}, 1600 rpm, O_2) were carried out in 0.5 M H_2SO_4 at room temperature. Further investigations of electrochemical stability were tested by two individual test protocols as follows.

- PCT (potential cycling test) for carbon corrosion test: 6,000 cycles, 1.0–1.6 V vs SHE, scan rate 100 mV s^{-1} at 25 °C.
- AST (accelerated stability test) for platinum dissolution test: 30,000 cycles, 0.6–1.0 V vs SHE, scan rate 100 mV s^{-1} at 25 °C.

The alterations were recorded by following aforementioned CV and LSV method after the PCT, and after AST for every 1 k, 3 k, 10 k, 20 k, 30 k cycles. These durability tests were adapted from many reported papers that conduced accelerated testing techniques [23–25].

2.5. Performance test of single cell

To optimize the ratio of CNTs and evaluate the single cell performances, the synthesized catalysts were used for the cathode and 40 wt.% Pt/C (HISPEC 4000, A Johnson Matthey) catalyst was used for the anode. The catalyst slurry was prepared by mixing each catalysts with Nafion solution (5 wt.% in lower aliphatic alcohols and water, 1100 EW) in isopropyl alcohol (Duksan). It was stirred for 5 min and sonicated for 3 min, which was repeated three times. The catalyst ink was sprayed on 1 cm^2 of Nafion 212 membrane with the platinum loading of 0.4 mg cm^{-2}. Then, Membrane Electrolyte Assembly (MEA) was fabricated with gas diffusion layer (SGL 10BC) [26,27]. The PEMFC single cell was operated under 75 °C and humidified to 100% RH by a vaporized H_2O gas. The gas flow rate of

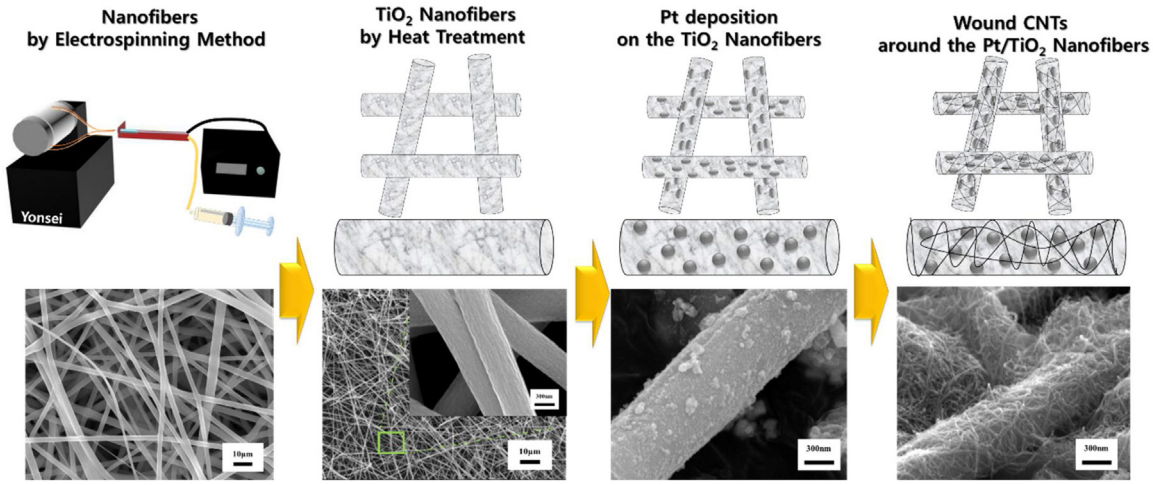

Scheme 1. Schematic diagram of CNT-Pt/TiO_2 nanofibrous catalyst fabrication procedure and SEM images. From left, each images indicates PVP/Ti, TiO_2, Pt/TiO_2, and CNT-Pt/TiO_2 nanofibers.

H_2 and O_2 were 100 and 150 sccm, respectively, with a stoichiometry of 1/1.5 (H_2/O_2) without giving a back-pressure. At first, to hydration and stimulate the catalytic activity, an activation step is needed. After the activation step, polarization curves were measured by using DC electrode load (6060B, Hewlett Packard). Also, at the same condition, electrochemical impedance spectroscopy (VSP, BioLogic) was applied to obtain the information of contact and interfacial resistance over the frequency range of 0.1–10,000 Hz. After then, O_2 gas was changed to N_2 gas to evaluate the catalytic behaviour of the electrode. When O_2 gas concentration had decreased, cyclic voltammetry was carried out analyzing at 50 mV s^{-1} and potential of 0 V to 1.2 V vs RHE.

A single cell test for high temperature and low humidity condition was conducted at 120 °C and humidified to 40% RH with MEA fabricated with Aquivion membrane (Short-side-chain PFSA). In the previous study, the Aquivion membrane shows better stability at high temperature [28]. The flow rates of H_2 and O_2 were 200 and 300 sccm. All the other procedures were exactly the same with the aforementioned test condition. Comparing to the commercial Pt/C, single cell durability test was conducted by constant voltage method at fixed operation condition of 0.6 V during 100 h.

3. Results and discussion

3.1. The synthesis and analysis of nanofibrous CNT-Pt/TiO_2 composite

The nanofibrous catalysts structure was prepared by the following procedure in Scheme 1. We prepared TiO_2 nanofibrous webs via electrospinning method under a carefully controlled condition. The electrospun nanofibers were thermally treated in air atmosphere to remove the PVP (Poly vinyl pyrrolidine) and to produce TiO_2 phase at the same time. Using this TiO_2 nanofibers as a support, Pt nanoparticles were well deposited on the nanofiber surfaces by the microwave-assisted polyol process. From the SEM-EDS in Fig. S1, the Pt loading was confirmed with nearly 40 wt.% as we designed for the Pt/TiO_2. To induce a sufficient electric conductivity and modify the electronic metal structure, ionomer-like structured carbon nanotubes (CNTs) were winded around the Pt/TiO_2 nanofibers. As observed from the SEM images in Scheme 1, the production process of the introduced catalysts is obviously verified. Electrospun PVP/Ti nanofibers were uniformly obtained with the average fiber diameter of 3–5 μm. These shrunk to about 10 times smaller size of around 300–500 nm after heat treatment due to the combustion of polymer and solvent. Even though deposition procedure of Pt nanoparticles on the TiO_2 surface was carried out, the nanofibrous web structure was retained to its original morphology. After finely treating CNT around the fibers, we could obtain the expected nanofibrous composite feature of CNT winded Pt/TiO_2 catalyst.

To observe the morphology of Pt nanoparticles on TiO_2 surface, HR-TEM images of Pt/TiO_2 nanofibers were displayed in Fig. 1(a–c). It was obviously seen that spherical Pt nanoparticles with an average size of 4.5 nm were well-deposited on the TiO_2 nanofibers surface. Generally, 3–5 nm is generally known to be a suitable size for an ORR electrocatalyst in PEMFC [29]. This size was also confirmed from calculation by XRD data with Scherrer's equation in Fig. 1(d). The TiO_2 and Pt can also be distinguished by lattice spacing of 0.353 nm corresponds to the (101) planes of anatase TiO_2 and 0.226 nm corresponds to the (111) plane of Pt.

Fig. 1(d) shows the XRD patterns of TiO_2, Pt/TiO_2 and CNT-Pt/TiO_2 nanofibers. The diffraction peaks of TiO_2 nanofibers show exactly same positions as an anatase phase at 2θ of 25.2°, 37.7°, 48.0°, 53.8°, 62.5°, 68.7° and 74.9°, correspond to (101), (004), (200), (105), (204), (116) and (215) crystal faces (JCPDS card no. 21–1272) with a space group of *I*41/amd. In the obtained TiO_2 anatase phase, the electron can move further faster for better performance than another TiO_2 phases. This properties are from the indirect band gap that enables excited electron to stabilize at lower level in conduction band itself, leading to its longer life and greater mobility [30]. After Pt deposition on the surface of TiO_2 nanofibers, XRD peaks for Pt metal was observed at 39.6° (111), 46.1° (200) and 67.7° (220) (JCPDS card no. 04-0802) while the TiO_2 phase did not change. And the presence of CNT around the TiO_2 nanofiber is inferred not only from the significant intensity decrease of the peaks but also from the peaks at 2 θ of 26.3° and 43.5° that refer to the (002) and (200) planes of CNTs. This indicates a fine formation of the CNT-Pt/TiO_2 nanofiber composite. Interestingly, Pt (111) plain peak of Pt/C, normally, places at 39.8°, while the Pt (111) peak of CNT-Pt/TiO_2 places on 39.6° [31]. From the Bragg's law, decrement of θ means Pt's d-space has increased and Pt particles on the surface has strained. It may be resulted from a strong interaction among the ternary system of Pt, TiO_2 support, and CNT for a change in the Pt chemical state. So, it is expected that TiO_2 nanofiber support may suppress the dissolution of Pt particles.

For studying more about the interaction of each materials, we performed X-ray photoelectron spectroscopy (XPS) and X-ray absorption spectroscopy (XAS) analysis of Ti 2p, O 1s, and C 1 s for

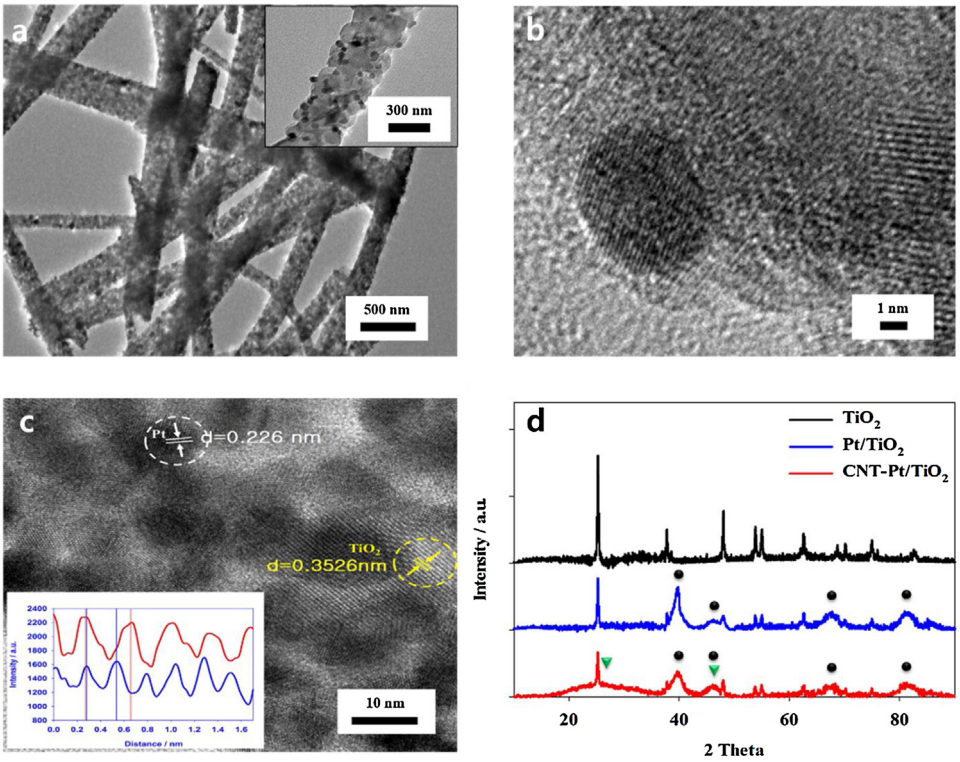

Fig. 1. (a)–(c) TEM images of Pt/TiO_2 nanofibers at different magnitude (inset at (c): lattice parameters of Pt and TiO_2) and (d) XRD patterns for TiO_2, Pt/TiO_2, CNT-PT/TiO_2.

CNT, TiO_2, Pt/TiO_2, CNT-Pt/TiO_2 and commercial Pt/C to investigate changes in chemical states. Ti 2p peaks of TiO_2, Pt/TiO_2, CNT-Pt/TiO_2 are shown in Fig. 2(a) for the binding energies of Ti $2p_{3/2}$ and $2p_{1/2}$. The position and shape of these peaks correspond to a perfect anatase TiO_2 as confirmed from XRD. However, the binding energy shifted to higher value when Pt was deposited, and even more when the CNT was additionally modified. The inset in Fig. 2(a) shows a same trend in the result of the O 1 s with a similar value. The higher binding energy can reflect an charge transfer between Pt, CNT and TiO_2, indicating a strong bonding with each materials by the SMSI effect [14,15,32,33]. Additional evidence for this synergistic effect was seen by XAS, encompassing X-ray absorption near edge structure (XANES) in Fig. 2(b). Comparing to the reference of TiO_2 (anatase), Ti $L_{II,III}$-edge ($2p \rightarrow 3d$) XAS spectra of the Pt/TiO_2 and CNT-Pt/TiO_2 show exactly the same position and shape [14,34,35]. Only the peak intensity was higher for the composite catalysts. The higher intensity of the absorption edge was proportional to the d-electron vacancies, which is also seen in the XAS spectra of the O K-edge in the inset of Fig. 2(b). It proved an electron donation from TiO_2 to Pt and CNT, explaining directly the SMSI effect. This kind of metal-support interaction can adjust the electronic and catalytic properties of the catalysts from the activation of the dispersed metal, which is significantly necessary for an efficient electrocatalytic system [33]. Therefore, Pt metal contacted with the TiO_2 nanofiber and additional CNT can be improved to an active phase with better charge transfer for higher catalytic activity.

To achieve an understanding for the details about the geometric structure and electronic properties of Pt in CNT-Pt/TiO_2 catalyst, XANES spectra of Pt L-edge and XPS spectra of Pt were performed. The XANES region of Pt L-edge was shown in Fig. 3(a) comparing to the plots of Pt foil, commercial Pt/C, Pt/TiO_2 and CNT-Pt/TiO_2. The intensities of the white-line around 11568 eV, corresponds to a $2p_{3/2}$ to 5d transition, were gradually decrease in the order of Pt foil, commercial Pt/C, Pt/TiO_2 and CNT-Pt/TiO_2 [34]. Generally, the white-line intensity can be affected by the particle sizes

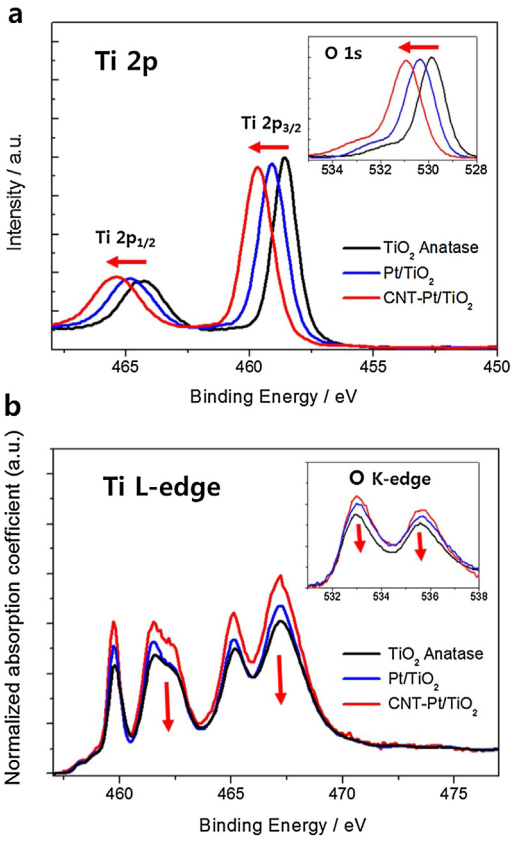

Fig. 2. (a) XPS spectra of Ti 2p (inset: O 1s) and (b) XAS spectra of Ti L-edge (inset: O K-edge) for TiO_2, Pt/TiO_2, and CNT-Pt/TiO_2 samples.

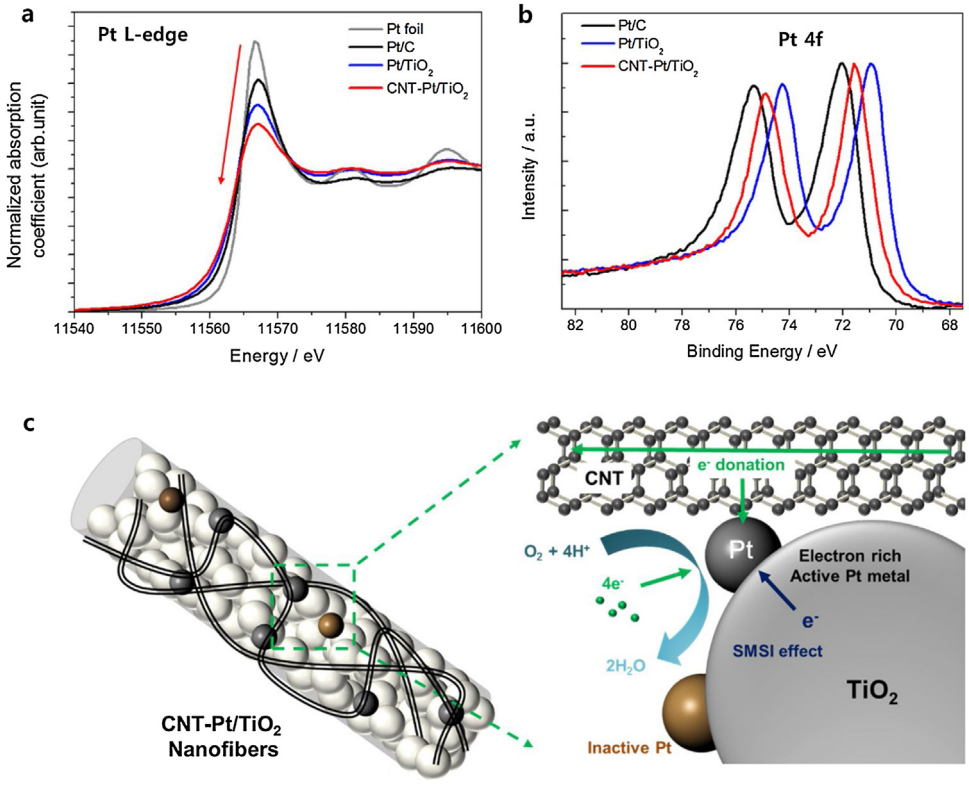

Fig. 3. (a) Normalized Pt L_{III} edge XANES spectra, (b) XPS spectra of Pt 4f, and (c) schematic illustration of the Pt chemical state for Pt/C, Pt/TiO_2 and CNT-Pt/TiO_2.

and/or electronic structure such as d-band vacancy. At this point, because we have similar particle sizes of Pt for all samples, the decreased intensity may mean a change in d-band vacancy of Pt. In the case of Pt/C and Pt/TiO_2, the decrease in intensity for Pt/TiO_2 can be understood as higher electron transfer from Ti to Pt than from carbon to Pt, resulting an high electron density around the Pt atoms, and hence a decrease in the Pt d-band vacancy due to the SMSI effect [15,16,33,36,37]. Fascinatingly, the white-line intensity further decreases when CNT was modified around the Pt/TiO_2 nanofiber. This transition might come from the electrons that are donated by CNTs. When the CNTs contact with other substrates, there is generally an electron transport which can induce changes of the chemical states [33,37,38]. This can lead to an extreme decrease in the d-band vacancy of Pt, which is normally determined as a number of unfilled d states [39]. We can predict that the CNT-Pt/TiO_2 nanofiber catalyst has the lowest number of unfilled d states for Pt by the synergy effect with CNT and TiO_2 nanofiber. The change in the d-band of the surface Pt atoms results in better catalytic activity by reducing the adsorptive strength of intermediates for higher ORR performance.

This new catalytic structure of Pt is also confirmed by the XPS spectra results. Shortly, Fig. 3(b) shows a slightly lower binding energy shift of Pt 4f of Pt/TiO_2 compared with Pt/C and the commensurate higher binding energy shift of Pt 4f of CNT-Pt/TiO_2 compared with Pt/TiO_2. It resulted from the strong interactions including a SMSI effect between Pt nanoparticles and TiO_2 nanofiber as we discussed before. The Pt 4f core peaks at 71.88 eV for Pt/C, at 70.58 eV for Pt/TiO_2, and 71.58 eV for CNT-Pt/TiO_2 catalyst show that all the deposited Pt are mainly in metallic state (Table 1). The Pt-O and Pt-OH bonding that could influence to the reduced ORR activity are generally higher for Pt on oxide supports like seen in Pt/TiO_2 than the Pt/C. However, the amount of Pt-O and Pt-OH was smaller and more metallic Pt was observed when CNTs were winded around the Pt/TiO_2 nanofiber catalyst. Therefore, we could obtain a new

Table 1
The peak position and chemical state of the loaded Pt in Pt/C, Pt/TiO_2 and CNT-Pt/TiO_2 from XPS analysis.

	Peak	Ratio%			
	eV	Pt	PtO_2	PtO	$Pt(OH)_4$
Pt/C	71.88	48.2	37.8	7.7	6.3
Pt/TiO_2	70.98	43.8	39.1	8.3	8.9
CNT-Pt/TiO_2	71.58	50.2	37.6	7.9	4.3

catalyst structure from all the characterization results as illustrated in Fig. 3(c). For the electronic structure point of view, the d-state of Pt is filled to be an active metal by the electron from the TiO_2 nanofiber and additional electron from the CNTs. Furthermore, the chemical structure of Pt particles changed to the relatively high metallic active phase by contacted CNTs on the surface of TiO_2 nanofiber. This modified structure is expected to increase the active sites of Pt and enhance the ORR activity as well as the durability for the PEMFC operation [16,40,41].

To evaluate the ORR activity, Fig. 4(a) displayed the polarization curves for commercial Pt/C, CNT, TiO_2 and CNT-Pt/TiO_2 nanofibers, which were obtained in O_2 saturated 0.5 M H_2SO_4 solution using a RDE at 1600 rpm and a rate of 50 mV s^{-1}. As we can expect, the plain TiO_2 nanofiber and CNT show almost no activity for ORR due to their absence of the catalytic active sites. After the Pt deposition on the TiO_2 nanofiber, we were able to see a reasonable activity with the onset and limiting current density of 0.85 V and -4.10 mA cm^{-2}, respectively, which may be resulted from nanofibrous structure and uniformly deposited Pt nanoparticles with the small size. As predicted, the ORR activity highly increased to the onset and limiting current density of 0.92 V and -4.60 mA cm^{-2} by the enhanced conductivity and electro catalytic structure through CNT modification. This value was even better than the result of the commercial 40% Pt/C.

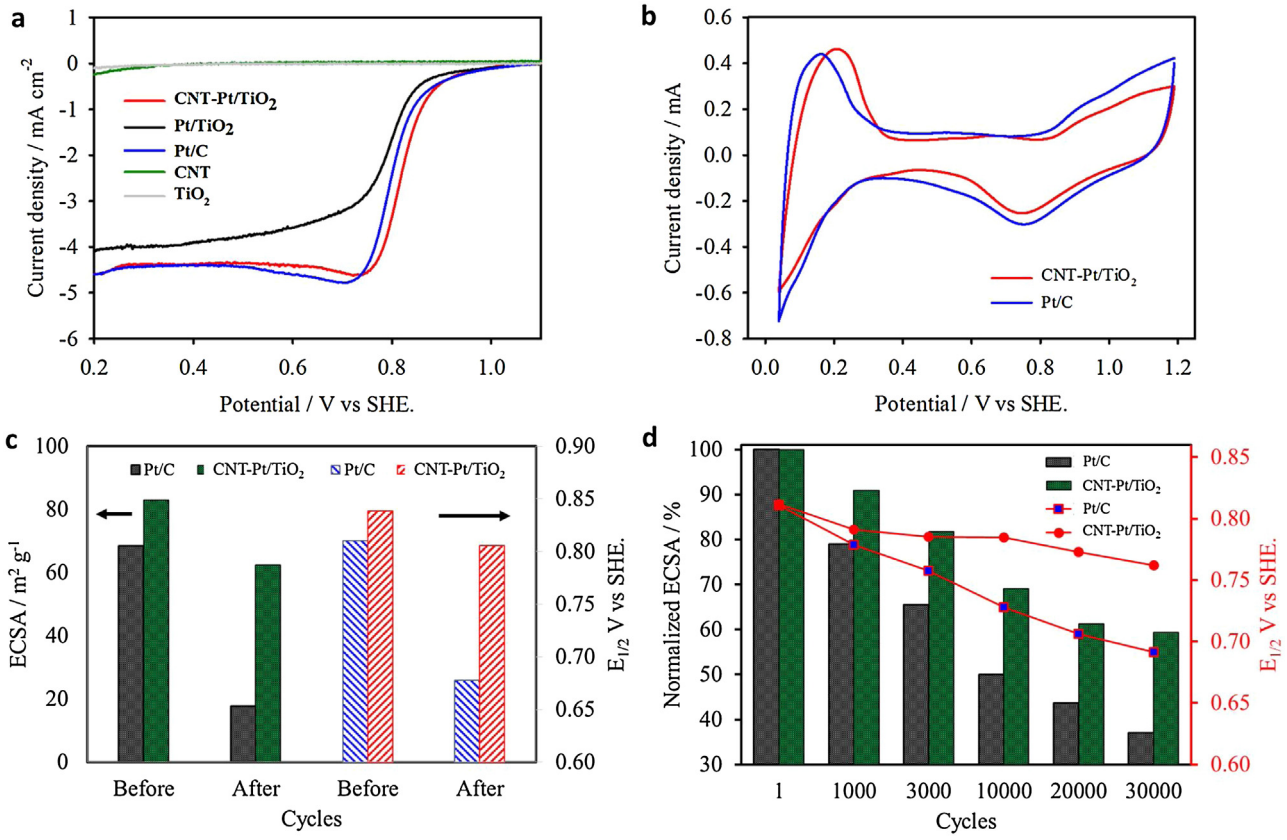

Fig. 4. The initial (a) cyclic voltammetry curves and (b) polarization curves as well as the comparison of the ECSAs and half-wave potentials after (c) PCT for 1,000 cycles and after (d) AST experiments for every 1 k, 3 k, 10 k, 20 k, 30 k cycles during 30,000 cycles in N_2 saturated 0.5 M H_2SO_4 solution.

We were also able to confirm this improved catalytic properties in Fig. 4(b) by the electrochemical surface area (ECSA) calculated from the shape of CV curves in N_2 saturated 0.5 M H_2SO_4 solution. The H_2 adsorption, desorption and O_2 adsorption, desorption peaks are clearly observed, and no additional current peaks were detected. This means CNT added Pt/TiO_2 is electrochemically inert to be a good support under PEMFC condition. Generally, the catalysts have high activity on the electrochemical reaction when the H_2 desorption area of CV is wider. It can be easily seen that CNT-Pt/TiO_2 nanofiber composite shows high activity compare to the activity of the commercial Pt/C. The ECSAs of Pts at CNT-Pt/TiO_2 nanofiber and Pt/C were obtained by the following Eq. (1) and the integration of the H_2 desorption peak into the amount of Pt used in the cathode.

$$(ECSA = \frac{Q_H}{mq_H}) \quad (1)$$

Q_H is the charge for H_2 adsorption, m is the amount of metal loading, and q_H of 210 mC cm^{-2} is the charge required for the monolayer adsorption of H_2 on Pt surfaces [8].Finally, we could calculate the ECSAs values of 85.69 m^2 g^{-1} and 67.31 m^2 g^{-1} for the CNT-Pt/TiO_2 nanofiber and Pt/C, respectively, showing the better electrochemical activity as also proved in the ORR results.

Surprisingly, the introduced CNT-Pt/TiO_2 nanofiber composite catalyst revealed not only a higher catalytic activity but also a much better durability under H_2SO_4 at the applied protocols. Two different protocols were used in this study to investigate the stability of different materials. Firstly, PCT protocols for CNT-Pt/TiO_2 nanofiber and commercial Pt/C were carried out at the potential range of 1.0–1.6 V where the carbon corrodes. As shown in Figs. S2(a) and S2(b), we could easily see that the CV shape of the Pt/C changed more than the CNT-Pt/TiO_2 nanofiber after the PCT. These trend can be confirmed from the change of the calculated ESCA values in Fig. 4(c). The ECSA of the CNT-Pt/TiO_2 catalyst was reduced to 76% of the original value whereas commercial Pt/C showed 26% of initial ECSA. Moreover, the half-wave potentials were compared at the ORR polarization curves in Fig. S2(c). These half-wave potentials before and after the durability tests were summarized in Fig. 4(c). The initial values for CNT-Pt/TiO_2 and Pt/C were 0.84 V and 0.81 V, after then these degraded to 0.81 V and 0.68 V, respectively. This improved stability of the CNT-Pt/TiO_2 nanofiber catalyst can be because TiO_2 nanofibers basically offer no corrosion and are very stable under such conditions. Although CNT-Pt/TiO_2 catalyst has a potentially corrosive carbon species, it is widespread knowledge that the graphitic carbon species endure better for the carbon corrosion than the disordered carbon support like Vulcan.

Fig. 4(d) is the ECSA results from the AST protocol with the potential range of 0.6–1.0 V to evaluate the degradation through platinum dissolution. The changes of ECSAs were calculated from the CV analysis in Figs. S3(a) and S3(b) during 30,000 cycles. In the case of commercial Pt/C, the ECSA value dropped almost 20% after the first 1000 cycles, and then steadily decreased to 37% of its original ECSA value. On the other hand, CNT-Pt/TiO_2 exhibited not only a higher ECSA value but also more stable behaviour. A steady decrease in the ECSA was observed, but the total ECSA loss was less than 40%. Furthermore, as from the polarization curves in Figs. S3(c) and S3(d), a similar degradation tendencies of each samples were revealed during the platinum dissolution tests. At the end of the AST, half-wave potential dropped to 0.76 V for the CNT-Pt/TiO_2 nanofiber catalyst and 0.69 V for the Pt/C catalyst from the initial values, which can be satisfying the suggestion of strong SMSI effect of the CNT-Pt/TiO_2 for the platinum dissolution test in sub scale.

To support these results, TEM analysis before and after both of the load-cycling protocols was performed in Fig. S4. In general,

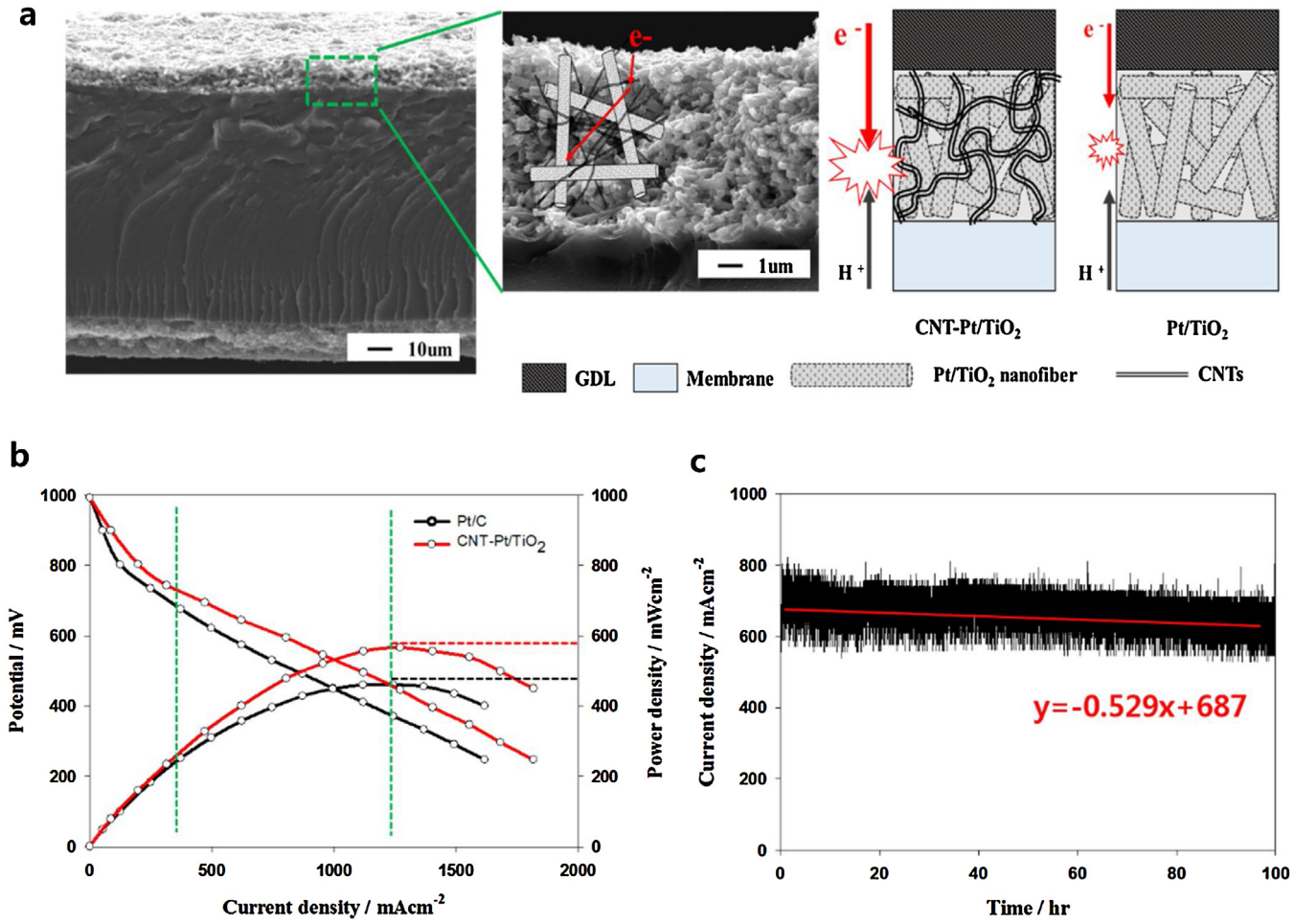

Fig. 5. (a) SEM images of MEA cross section at different magnitude with its schematic illustration of the expected advantage in nanofibrous electrode, (b) I–V curves and (c) durability test of the CNT-Pt/TiO_2 according to the current density (mA cm^{-2}) along with time (hour) at constant voltage mode of 0.6 V for high temperature single cell test (T_{cell} = 120 °C, RH 40%).

the Pt size grows where the carbon support corrosion take place and this phenomenon was obviously shown after the PCT with an increase from 4.2 nm to 7.9 nm. As the TiO_2 based support does not have any corrosion, the Pt on the CNT-Pt/TiO_2 catalysts was quite stable with almost no change of 5–6 nm. In the case of the AST experiments, the Pt size is more about the Pt and support interaction to alleviate the Pt dissolution. We could simply notice the difference at a glance that the average particle size of commercial Pt/C was significantly affected with a large increase from 4.2 nm to 8.1 nm. However, there is no distinctive varies in CNT-Pt/TiO_2 nanofiber catalyst with only a change from 5.1 nm to 6.1 nm, which was absolutely due to the favourable interfacial bonding structure between Pt and TiO_2 support that alleviates the Pt growth. These all results confirm that the electrochemical Ostwald ripening and carbon corrosion are predominant in an operating potential region, it threaten the long term operation of Pt/C based catalyst. As a result, we found that it can reduced by using alternative support material like our CNT-Pt/TiO_2 nanofibrous catalyst, which will be also efficient to the single cell operation.

3.2. PEMFC single cell performance of CNT-Pt/TiO_2

To perform single cell tests, MEAs were fabricated with nanofibrous cathode that is composed by the prepared CNT-Pt/TiO_2 nanofiber catalyst. From the SEM image of the MEA cross-section in Fig. 5(a), cathode layer was around 7 μm thick including a perfectly stacked nanofibrous web with an enhanced pore structure. The thickness was smaller than the Pt/C based cathode (Fig. S5) due to the higher density of TiO_2 nanofiber, which can be also an important factor of short mass transfer pathway. Especially, well-modified CNTs were also clearly observed where CNT can act as a bridge for electrical pathway with maintaining nanofibrous structure. As illustrated in Fig. 5(a), this enables electrons that occurred from anode transfer to cathode while TiO_2 based cathode cannot [42,43].

Fig. S6(a) shows the I–V curves of the single cell tests at T_{cell} = 75 °C, RH 100% for the CNT-Pt/TiO_2 nanofiber catalysts with different CNT ratios. As we expected, the CNT modified Pt/TiO_2 nanofiber catalysts shows more than 9 times higher performance than the Pt/TiO_2 by the improved electron transfer and Pt active phase. The change in the charge transfer resistance of the cell in Fig. S6(b) can prove this effect. It decrease from 1.11 Ω to maximum 0.189 Ω at 0.6 V that is almost 6 times smaller. H_2 desorption peak from the CV in Fig. 6S (c) also shows an enlarged area where the ECSAs are increase from the 9.52 m^2 g^{-1} for Pt/TiO_2 to maximum 20.46 m^2 g^{-1} for 10 wt% CNT-Pt/TiO_2. We can describe that CNT makes suitable electrical pathways lead to not only reduce the resistance of TiO_2 but also enlarge the triple boundary phase (TBP) with more active Pt particles. However, according to changes by different CNT ratios, overusing of CNTs might cover the active sites and hinder the oxygen transfer. Also, it could lengthen the electrical pathway that can cause the electrical resistance. These were able

Table 2
The performance and durability results for the Pt/C (Fig. S7) and CNT-Pt/TiO_2 nanofiber catalysts (Fig. 5) at HT-PEMFC operation conditions of 120 °C and RH 40%.

	Open circuit voltage	Current density (0.6 V)	Performance Degradation (y = −ax + y0)	
	V	mA cm^{-2}	a	y0
Pt/C	0.993	562	0.648	549
CNT-Pt/TiO_2	0.997	781	0.529	687

to observe in the mass transfer region and i-R region. As a result from Fig. S6(a), among these CNT modified catalysts, the Pt/TiO_2 nanofiber catalyst modified with 10% of CNT reveals the optimum performance of 1488 mA cm^{-2} at 0.6 V and maximum power density of 0.89 W cm^{-2}, which is comparable to the commercial Pt/C. This high value may came from well-designed electrode by the CNT-Pt/TiO_2 nanofiber catalysts which with high electrochemical activity and enhanced pore structure for better mass transfer.

This new fine nanofibrous structure is expected to be much more favourable to the PEMFC operation at higher temperature due to the active and stable properties of the TiO_2 nanofibers than the original carbon supports. In Fig. 5(b), we conducted single cell tests to verify whether the catalyst has possibility to use for HT-PEMFC at 120 °C and RH 40%. For the MEA fabrication, Aquivion commercial membrane was used instead of Nafion membrane since Aquivion membrane was proved to reveal a better performance and stability at high temperature from our previous work [28]. Fig. 5(b) shows the I–V curves for the CNT-Pt/TiO_2 nanofiber and commercial Pt/C catalysts to compare the performance at high temperature. As listed in Table 2, both OCVs were similar due to the use of the same Aquvion membrane. Overall, it was a general phenomenon that the performance decreases when the temperature goes up to over 80 °C and the relative humidity goes down to 40%, leading to a decline of proton conductivity of the membrane/ionomer [10,43]. Furthermore, a Pt nanoparticle growth can be accelerated at high temperature due to the faster dissolution rate including carbon corrosion. However, the obtained performance of CNT-Pt/TiO_2 nanofiber catalyst reveals even higher value for current density of 781 mA cm^{-2} at 0.6 V and maximum power density of 567 mW cm^{-2} than the commercial Pt/C with a value for current density of 562 mA cm^{-2} at 0.6 V and maximum power density of 461 mW cm^{-2}. Remarkably, the introduced catalyst displayed a better performance at all three regions of kinetic region (OCV–0.75 V), ohmic polarization region (0.75–0.40 V), and mass-transfer-controlled region (0.40–0.20 V) as divided in Fig. 5(b). As the kinetic region is primarily influenced by the ORR activity of the catalyst, CNT-Pt/TiO_2 nanofiber catalyst shows improved activity due to its enhanced electrical structure of Pt by the strong interaction with TiO_2 support and CNT (Fig. 3(c)). Moreover, TiO_2 may also encourage more to the catalytic activity at high temperature from the original properties of oxide materials. The higher limiting current density at low voltage in mass-transfer-controlled region is generally limited by the transport of reactant gas for the catalytic reactions in the cathode and illustrates the effectiveness of mass transfer of the reactant. While oxides such as TiO_2 have small surface area, the nanofibrous structure in our study provides a 3D open pore configuration with higher surface area for better mass transfer at the electrode. To sum up both, a higher performance at ohmic polarization region were achived for the CNT-Pt/TiO_2 nanofiber catalyst.

In addition, the durability of the CNT-Pt/TiO_2 nanofiber catalyst was much more distinguishable compare to the commercial Pt/C catalyst. As the HT-PEMFC condition is not appropriate to conduct the half-cell test, constant durability MEA tests at 0.6 V for 100 h were carried in Fig. 5(c), same as our previous work [28]. With even higher initial current density than Pt/C, outstanding durability was obtained with a minor grade of linear regression (Table 2). This value was reasonable at the severe operating conditions of high temperature and low humidity whereas an obvious decay of the Pt/C slope in Fig. S7 was seen at many regions due to the material degradations. Therefore, we can say that our designed nanofibrous structure by modifying CNTs to Pt/TiO_2 nanofibers can be an innovative approach in making an active and durable catalyst for the PEMFC operation at high temperature.

4. Conclusion

In summary, we fabricated a newly designed nanofibrous electrode using CNT-Pt/TiO_2 nanofiber catalyst to replace a widespread platinum supported on carbon catalyst that can be seriously corroded in HT-PEMFCs operation condition. In order of precedence, the Pt nanoparticles were deposited on TiO_2 surface and ionomer-like structured CNTs was entangled to the Pt/TiO_2 nanofiber surfaces. We found that the introduction of TiO_2 nanofiber helped to a better durability due to the good stability itself and SMSI effect between the materials, which were confirmed by the PCT and AST experiments, respectively. Through adding CNTs into the electrode, the CNT-Pt/TiO_2 nanofiber catalyst provided better electrical pathway and leaded to a change in the electrochemical structure of surface Pt atoms that reduced the adsorptive strength of intermediates with an optimum TPB for higher ORR and MEA performance. As a result, CNT-Pt/TiO_2 nanofiber catalyst presented a significantly enhanced activity and durability compare to the commercial Pt/C catalyst at high temperature conditions of 120 °C and RH 40%. Therefore, we can insist that our nanofibrous electrode can be one of the promising candidates for high performance and stable cathode to open the area of HT-PEMFC.

Acknowledgments

This research was supported by the Technology Development Program to Solve Climate Changes of the National Research Foundation (NRF) funded by the Ministry of Science, ICT & Future Planning (NRF-2015M1A2A2056833).

Appendix A. Supplementary data

Supplementary data associated with this article can be found, in the online version, at http://dx.doi.org/10.1016/j.apcatb.2016.11.053.

References

[1] H.A. Gasteiger, N.M. Markovic, Science 324 (2009).
[2] P. Trogadas, T. Fuller, A. Franco, Polymer Electrolyte Fuel Cells: Science, Applications and Challenges, CRC Press/Taylor and Francis group, Boca Raton, FL, 2013.
[3] K.A. Mauritz, R.B. Moore, Chem. Rev. 104 (2004) 4535–4586.
[4] A. Parthasarathy, S. Srinivasan, A.J. Appleby, C.R. Martin, J. Electrochem. Soc. 139 (1992) 2530–2537.
[5] S. Sharma, B.G. Pollet, J. Power Sources 208 (2012) 96–119.
[6] S.G. Chalk, J.F. Miller, J. Power Sources 159 (2006) 73–80.
[7] Z. Siroma, K. Ishii, K. Yasuda, Y. Miyazaki, M. Inaba, A. Tasaka, Electrochem. Commun. 7 (2005) 1153–1156.
[8] M.S. Wilson, F.H. Garzon, K.E. Sickafus, S. Gottesfeld, J. Electrochem. Soc. 140 (1993) 2872–2877.
[9] P. Su-Il, L. Eung-Jo, K. Tae-Young, L. Seo-Jae, R. Young-Gyoon, K. Chang-Soo, Carbon 32 (1994) 155–159.
[10] Y. Shao, G. Yin, Z. Wang, Y. Gao, J. Power Sources 167 (2007) 235–242.
[11] K. Sasaki, F. Takasaki, Z. Noda, S. Hayashi, Y. Shiratori, K. Ito, ECS Trans. 33 (2010) 473–482.
[12] D.P. Macwan, P.N. Dave, S. Chaturvedi, J. Mater. Sci. 46 (2011) 3669–3686.
[13] U. Diebold, Appl. Phys. A: Mater. Sci. Proc. 76 (2003) 681–687.
[14] N.G. Akalework, C.-J. Pan, W.-N. Su, J. Rick, M.-C. Tsai, J.-F. Lee, J.-M. Lin, L.-D. Tsai, B.-J. Hwang, J. Mater. Chem. 22 (2012) 20977.

[15] V.T. Ho, C.J. Pan, J. Rick, W.N. Su, B.J. Hwang, J. Am. Chem. Soc. 133 (2011) 11716–11724.
[16] A. Lewera, L. Timperman, A. Roguska, N. Alonso-Vante, J. Phys. Chem. C 115 (2011) 20153–20159.
[17] D. Li, Y. Xia, Nano Lett. 3 (2003) 555–560.
[18] H. Li, W. Zhang, W. Pan, A. Agrios, J. Am. Ceram. Soc. 94 (2011) 3184–3187.
[19] Y.T. Sung, M.S. Han, K.H. Song, J.W. Jung, H.S. Lee, C.K. Kum, J. Joo, W.N. Kim, Polymer 47 (2006) 4434–4439.
[20] Q. Long, M. Cai, J. Li, H. Rong, L. Jiang, J. Nanopart. Res. 13 (2010) 1655–1662.
[21] L. Dennany, P. Sherrell, J. Chen, P.C. Innis, G.G. Wallace, A.I. Minett, Phys. Chem. Chem. Phys. 12 (2010) 4135–4141.
[22] F.-J. Lai, L.S. Sarma, H.-L. Chou, D.-G. Liu, C.-A. Hsieh, J.-F. Lee, B.-J. Hwang, J. Phys. Chem. C 113 (2009) 12674–12681.
[23] W. Schmittinger, A. Vahidi, J. Power Sources 180 (2008) 1–14.
[24] R.L. Borup, J.R. Davey, F.H. Garzon, D.L. Wood, M.A. Inbody, J. Power Sources 163 (2006) 76–81.
[25] R. Borup, J. Meyers, B. Pivovar, Y.S. Kim, R. Mukundan, N. Garland, D. Myers, M. Wilson, F. Garzon, D. Wood, Chem. Rev. 107 (2007) 3904–3951.
[26] C. Lee, S.M. Jo, J. Choi, K.-Y. Baek, Y.B. Truong, I.L. Kyratzis, Y.-G. Shul, J. Mater. Sci. 48 (2013) 3665–3671.
[27] Y.I. Cho, Y. Jeon, Y.-G. Shul, J. Power Sources 263 (2014) 46–51.
[28] Y. Jeon, S.m. Juon, H. Hwang, J. Park, Y.-g. Shul, Electrochim. Acta 148 (2014) 15–25.
[29] S.J. Yoo, T.Y. Jeon, K.S. Lee, K.W. Park, Y.E. Sung, Chem. Commun. (Camb) 46 (2010) 794–796.
[30] T. Luttrell, S. Halpegamage, J. Tao, A. Kramer, E. Sutter, M. Batzill, Sci. Rep. 4 (2014) 4043.
[31] Y.H. Chung, S.J. Kim, D.Y. Chung, M.J. Lee, J.H. Jang, Y.E. Sung, Phys. Chem. Chem. Phys. 16 (2014) 13726–13732.
[32] J.J. Palacios, A.J. Perez-Jimenez, E. Louis, E. SanFabian, J.A. Verges, Phys. Rev. Lett. 90 (2003) 106801.
[33] C.-K. Yang, J. Zhao, J.P. Lu, Phys. Rev. B 66 (2002).
[34] K. Huang, K. Sasaki, R.R. Adzic, Y. Xing, J. Mater. Chem. 22 (2012) 16824.
[35] S. Mukerjee, S. Srinivasan, M.P. Soriaga, J. McBreen, J. Electrochem. Soc. 142 (1995) 1409–1422.
[36] D. Sung, N. Park, J.-Korean Phys. Soc. 50 (2007) 708.
[37] Y. Xue, S. Datta, Phys. Rev. Lett. 83 (1999) 4844.
[38] I. Deretzis, A.L. Magna, Nanotechnology 17 (2006) 5063–5072.
[39] L. Timperman, A. Lewera, W. Vogel, N. Alonso-Vante, Electrochem. Commun. 12 (2010) 1772–1775.
[40] A. Talo, J. Lahtinen, P. Hautojärvi, Appl. Catal. B 5 (1995) 221–231.
[41] C.R. Parkinson, M. Walker, C.F. McConville, Surf. Sci. 545 (2003) 19–33.
[42] P. Lee, J. Lee, H. Lee, J. Yeo, S. Hong, K.H. Nam, D. Lee, S.S. Lee, S.H. Ko, Adv. Mater. 24 (2012) 3326–3332.
[43] C. Wieser, Fuel Cells 4 (2004) 245–250.